

Investigation of the structure and phase transitions in the novel A-site substituted distorted perovskite compound $\text{Na}_{0.5}\text{Bi}_{0.5}\text{TiO}_3$

G. O. Jones* and P. A. Thomas

Department of Physics, University of Warwick,
Coventry CV4 7AL, EnglandCorrespondence e-mail:
g.o.jones@warwick.ac.uk

Rietveld neutron powder profile analysis of the compound $\text{Na}_{0.5}\text{Bi}_{0.5}\text{TiO}_3$ (NBT) is reported over the temperature range 5–873 K. The sequence of phase transitions from the high-temperature prototypic cubic structure (above 813 K), to one of tetragonal (673–773 K) and then rhombohedral structures (5–528 K) has been established. Coexisting tetragonal/cubic (773–813 K) and rhombohedral/tetragonal (with an upper temperature limit of 145 K between 528 and 673 K) phases have also been observed. Refinements have revealed that the rhombohedral phase, space group $R3c$, with $a_H = 5.4887$ (2), $c_H = 13.5048$ (8) Å, $V = 352.33$ (3) Å³, $Z = 6$ and $D_x = 5.99$ Mg m⁻³, exhibits an antiphase, $a^-a^-a^-$ oxygen tilt system, $\omega = 8.24$ (4)°, with parallel cation displacements at room temperature. The tetragonal phase, space group $P4bm$, with $a_T = 5.5179$ (2), $c_T = 3.9073$ (2) Å, $V = 118.96$ (1) Å³, $Z = 2$ and $D_x = 5.91$ Mg m⁻³, possesses an unusual combination of in-phase, $a^0a^0c^+$ oxygen octahedra tilts, $\omega = 3.06$ (2)°, and antiparallel cation displacements along the polar axis. General trends of cation displacements and the various deviations of the octahedral network from the prototypic cubic perovskite structure have been established and their systematic behaviour with temperature is reported. An investigation of phase transition behaviour using second harmonic generation (SHG) to establish the centrosymmetric or non-centrosymmetric nature of the various phases is also reported.

Received 20 June 2001

Accepted 4 December 2001

1. Introduction

Sodium bismuth titanate ($\text{Na}_{0.5}\text{Bi}_{0.5}\text{TiO}_3$), NBT, is an A-site substituted distorted perovskite compound. A-site substituted perovskite compounds, rather than solid solutions, are much rarer than their B-site substituted counterparts. The small number of examples includes, in addition to NBT, its analogue $\text{Ag}_{0.5}\text{Bi}_{0.5}\text{TiO}_3$ (Park *et al.*, 1999), $\text{K}_{0.5}\text{Bi}_{0.5}\text{TiO}_3$ (Smolenskii *et al.*, 1960), $\text{Ag}_{0.5}\text{Nd}_{0.5}\text{TiO}_3$ (Park *et al.*, 1998) and the rare-earth manganites typified by $\text{La}_{0.5}\text{Sr}_{0.5}\text{MnO}_3$ (Woodward *et al.*, 1998). The study of these compounds offers an opportunity to investigate the structural influence and resulting properties when the A-site cations are the primary determining factor of the resulting structure.

Since the discovery of NBT (Smolenskii *et al.*, 1960) many of its characteristics, particularly optical and dielectric properties and structural phase transitions, have been studied (Suchanicz & Ptak, 1990; Tu *et al.*, 1994; Vakhrushev *et al.*, 1989). The fundamental sequence of phase transitions from the high-temperature prototypic cubic structure to a tetragonal phase at a temperature within the range 783–813 K and then a rhombohedral phase below a temperature of approxi-

mately 533 K was established by Suchanicz & Kwapulinski (1995). Other investigations have taken place (Suchanicz & Kwapulinski, 1995; Isupov & Kruzina, 1983), but definitive structure determinations have not been made. Recently, Soukhovjak *et al.* (2000) have shown that the tetragonal phase shows $a^0a^0c^+$ octahedral tilts, which agrees with the structure reported by Jones & Thomas (2000). These studies are in accordance with Vakhrushev's earlier assignment of this tilt system (Vakhrushev *et al.*, 1985) for the tetragonal phase. There still remains controversy concerning phase transition temperatures, the development of regions of coexistence of rhombohedral–tetragonal and tetragonal–cubic phases and their electric order. The actual symmetry and structure of the phases has also not been unambiguously established. Opinions concerning the properties in and above temperature regions between the tetragonal and rhombohedral phases also vary. From the present state of knowledge, the overall picture relating to structural phases, phase transition behaviour and physical properties is inconsistent and needs resolving.

In this paper a comprehensive neutron powder diffraction study of the crystal structure and successive structural phase transitions occurring in NBT in the temperature range 5–873 K is reported. The results of Rietveld profile refinements, observed superstructure reflections and tilt systems as well as octahedral distortions, cation displacements and space-group assignment for the different phases are discussed. The unusual combination of tilts and cation displacements exhibited in the tetragonal phase, previously presented by Jones & Thomas (2000), is also discussed in greater detail. For the first time measurement of second harmonic generation as a function of temperature of NBT and results of low-temperature neutron powder diffraction are reported. The overall sequence of phases and structures for NBT is clarified.

2. Experimental

2.1. Sample preparation

NBT crystals were grown *via* spontaneous crystallization from the flux in closed platinum crucibles in air. The starting materials consisted of reagent-grade powders (99.9% purity) of Na_2CO_3 , Bi_2O_3 and TiO_2 . Stoichiometric amounts were weighed and thoroughly mixed. The ground powders were then calcined in closed platinum crucibles for 12 h at 1073 K, re-ground and calcined again under identical conditions. The crystals were in the form of pale yellow parallelepipeds of size $\sim 1 \text{ mm}^3$. Phase characterization and composition were confirmed using X-ray powder diffraction with a Bruker D5005 diffractometer and microprobe chemical analysis. Powdered samples for neutron diffraction were obtained from ground crystals.

2.1.1. Neutron data collection. Powder neutron diffraction was undertaken to obtain accurate information about the oxygen fractional coordinates in the presence of bismuth and to avoid the problems of twinning in single-crystal studies. Neutron powder data were collected between 5 and 873 K on diffractometer D2B at the Institut Laue–Langevin (ILL). The

sample was loaded into a cylindrical vanadium canister (height 6 cm, diameter 1 cm). Low-temperature collections were made using a cryofurnace (1.5–300 K); data sets were collected at 5, 50, 100, 150, 200 and 250 K on heating. High-temperature collections were made using a furnace (200–1000 K); data sets were collected at 293, 400, 473, 528, 573, 593, 673, 698, 723, 773, 793, 813 and 873 K on heating. A wavelength of 1.594 \AA was used. A static sample 2θ scan was employed with 64 ^3He counting tubes as detectors. In each run intensities up to 2θ of approximately 160° , step size 0.05, were measured with data collection times typically being 4 h per temperature run.

2.1.2. Second harmonic generation (SHG). The SHG powder technique provides a sensitive test for non-centrosymmetry. It demonstrates whether the crystal symmetry contains a centre of inversion or not and so can be used to resolve certain space-group ambiguities. Using the experimental set-up and apparatus similar to that described by Kurtz & Perry (1968), the second harmonic signals in NBT were detected and measured. Polycrystalline powdered samples were sieved to give a known particle size range and encapsulated into glass cells suitable for high-temperature studies. After furnace calibrations and null checks were performed, the NBT samples were placed in a small furnace having apertures normal to the sample orientation (Fig. 1). Through the furnace aperture, an intense beam (100 mJ, 100 ms pulse) from a Q-switched Nd:YAG laser ($\lambda = 1064 \text{ nm}$) was incident on the sample. The scattered radiation was first filtered to remove traces of the fundamental beam and any second harmonic signal ($\lambda = 532 \text{ nm}$) detected using a photomultiplier and displayed as a signal *versus* time pattern on an oscilloscope. A beam splitter and photodiode were employed to monitor the fundamental beam, so corrections could be made for any variation in laser output. The entire experimental set-up was enclosed in a light-proof box.

3. Results

3.1. Rhombohedral phase: refinement and structural characterization

Refinements by the Rietveld profile fitting method with GSAS (Von Dreele & Larson, 1995) were carried out with the following neutron scattering lengths: Na 0.363, Bi 0.853, Ti -0.344 , O $0.581 \times 10^{-12} \text{ cm}$. Referring to the double unit-cell

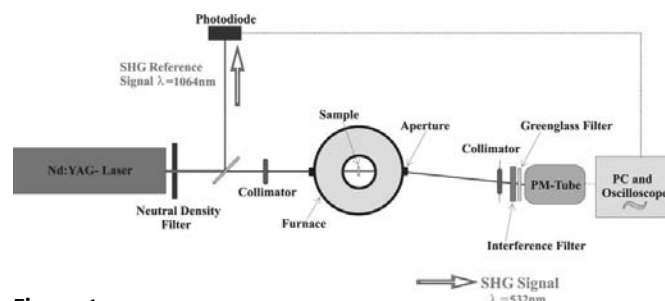


Figure 1
Schematic representation of the experimental set-up for powder SHG measurement as a function of temperature.

superstructure, reflections of the type h odd, k odd, l odd were observed within the temperature range 5–593 K. These were consistent with the $a^-a^-a^-$ tilt system (Glazer, 1975) seen in rhombohedral perovskites arising from oxygen octahedra tilting about their threefold pseudo-cubic axes. This tilt system is characterized by opposite rotations of adjacent octahedra along each axis, which consequently results in cell doubling of all three pseudo-cubic axes. A view of the structure down $[001]$ showing the tilt system is shown in Fig. 2. Rhombohedral perovskites are restricted to space groups $R3m$, $R\bar{3}c$ or $R3c$. The space groups $R3c$ and $R\bar{3}c$ can support tilt systems. $R3c$ has a polar symmetry permitting ferroelectricity, while $R\bar{3}c$ is non-polar, keeping the cation in the centre of inversion. The space group $R3m$ can be disregarded for NBT, because of the presence of superstructure reflections. Initial refinements of this phase were carried out in $R3c$ (the generally accepted space group for this phase) and based on the PZT model proposed by Corker *et al.* (1998). Models for each subsequent temperature were taken from the previous refinement.

As it is standard to describe the rhombohedral system on a rhombohedrally centred hexagonal lattice projected down the threefold axis, the rhombohedral structure is referred to on hexagonal axes, whose lattice parameters a_H and c_H are specified in relation to the double pseudo-cubic cell ($2a_p \times 2b_p \times 2c_p$) by the matrix:

$$\begin{pmatrix} 0.5 & 0 & -0.5 \\ -0.5 & 0.5 & 0 \\ 1 & 1 & 1 \end{pmatrix}.$$

Following the procedure originally developed by Megaw & Darlington (1975), this setting allows structural parameters to be readily defined and leads to the set of atomic fractional coordinates given in Table 1.¹

$R3c$ is characterized by cation displacements along $[111]_p$ combined with antiphase octahedral rotations. The room-temperature structure was refined in this space group. The background was based on a linear function and peak shapes described by pseudo-Voigt profiles. After preliminary refinements were made to establish parameters describing diffractometer characteristics and the scale factor, the remaining structural parameters were refined. As the space group $R3c$ allows an arbitrary choice of origin, in structural refinements the $O_{(z)}$ position was fixed to 1/12, see Table 1. Isotropic temperature parameters were initially refined followed by anisotropic parameters. Initially, Na and Bi, each with site occupation factor 0.5, were constrained to be at the same coordinates. As a check on the stoichiometry, the occupancies of Na^+ and Bi^{3+} were refined (given the constraint that the total occupancy should be 1) to values of 0.490 (7) and 0.510 (7), showing that any deviation from the ideal composition was small. The occupancies were subsequently fixed for the remaining refinements. The Na and Bi positions were then allowed to refine separately with the result that Bi became

¹Supplementary data for this paper are available from the IUCr electronic archives (Reference: OS0082). Services for accessing these data are described at the back of the journal.

Table 1

Fractional coordinates for hexagonal setting of $R3c$, in terms of independent refinable parameters.

s is the fractional shift of Na/Bi along c_H (or $[111]_p$); t the fractional shift of Ti along c_H (or $[111]_p$); d describes a distortion of the oxygen octahedron, keeping threefold symmetry, but making the upper and lower faces with respect to c_H different in size; e relates to the tilt of the octahedron about c_H and the angle of tilt ω is given by $\tan \omega = 4(3)^{1/2}e$.

Atom species	Site	x	y	z
Na/Bi	6(a)	0.00	0.00	$s + 0.25$
Ti	6(a)	0.00	0.00	t
O	18(b)	$1/6 - 2e - 2d$	$1/3 - 4d$	1/12

displaced 0.003 (2) Å along the polar axis (+ c) with respect to Na. Introducing this freedom had a negligible effect on the profile parameters and no effect on the anisotropic temperature factors. The Na and Bi positional parameters were constrained to the same positions for all further refinements. The refinement was stable and converged quickly. The crystallographic data and the refined profile parameters are summarized in Table 2. The observed, calculated and difference profiles from the final Rietveld refinement in $R3c$ are shown in Fig. 3(*a*). Subsequent refinements for rhombohedral phases taken at different temperatures were made (resulting in similar R factors as quoted for 293 K) and general trends in structural parameters investigated. Fig. 4 shows the variation in the rhombohedral lattice parameters as a function of temperature. Figs. 5(*a*) and 5(*b*) show the trend followed by the cation displacements as temperature is increased in this phase. Figs. 6(*a*) and 6(*b*) show the modification in the octahedral tilt angle and octahedron strain as a function of temperature, respectively. The variation of the octahedron

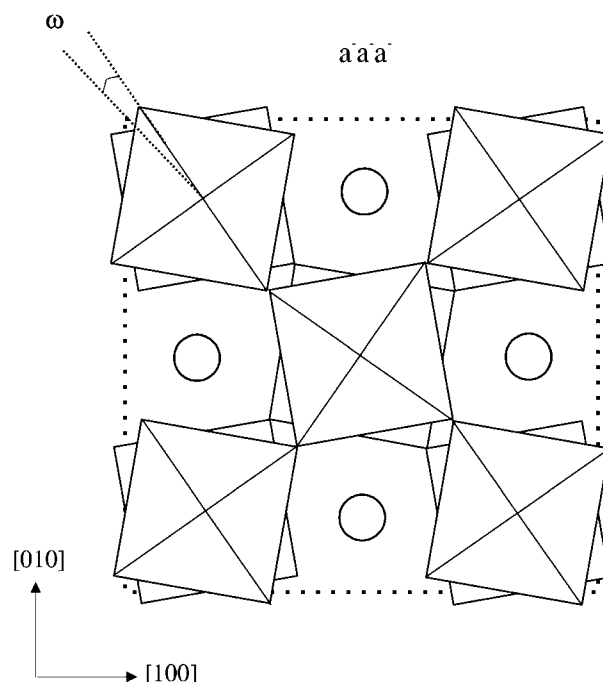


Figure 2

The projection of the rhombohedral structure down $[001]$; open circles represent Na/Bi sites.

Table 2

(a) Crystallographic data and (b) fractional coordinates and equivalent anisotropic displacement parameters (\AA^2) for NBT.

(a)

Chemical formula	$\text{Na}_{0.5}\text{Bi}_{0.5}\text{TiO}_3$		
Chemical formula weight	211.88		
Specimen shape	Random powder		
Specimen preparation	Crystal growth from flux, powder prepared from ground crystals		
Specimen pressure	Ambient		
Colour	Pale yellow		
Radiation type	Neutron		
Wavelength (\AA)	1.594		
Crystal system	Rhombohedral	Tetragonal	Cubic
Temperature (K)	293	673	873
Space group	$R3c$	$P4bm$	$Pm\bar{3}m$
a_H (\AA)	5.4887 (2)	–	–
c_H (\AA)	13.5048 (8)	–	–
a_p (\AA)	–	5.5179 (2)	3.91368 (3)
c_p (\AA)	–	3.9073 (2)	–
α, β, γ ($^\circ$)	90, 90, 120	90, 90, 90	90, 90, 90
α_p ($^\circ$)	89.83	–	–
Volume (\AA^3)	352.33 (3)	118.96 (1)	59.945 (5)
Z	6	2	1
D_x (Mg m^{-3})	5.99	5.91	5.87
s	0.0127 (6)	0.035 (1)	0.0
t	0.0063 (6)	–0.015 (4)	0.0
d	–0.0006 (3)	–	–
e	0.0209 (1)	–	–
Tilt system	$a^- a^- a^-$ (three tilt system, antiphase)	$a^0 a^0 c^+$ (one tilt system, in-phase)	$a^0 a^0 a^0$ (zero-tilt system)
Displacements	Parallel along $[111]_p$	Antiparallel along $[001]$	None
ω ($^\circ$)	8.24 (4)	3.06 (2)	0.0
$\zeta \times 10^2$	–0.589 (8)	–	–
No. of refined parameters	42	43	39
Profile R factors			
R_p	0.059	0.044	0.045
wR_p	0.078	0.056	0.053
χ^2	0.323	0.786	0.710

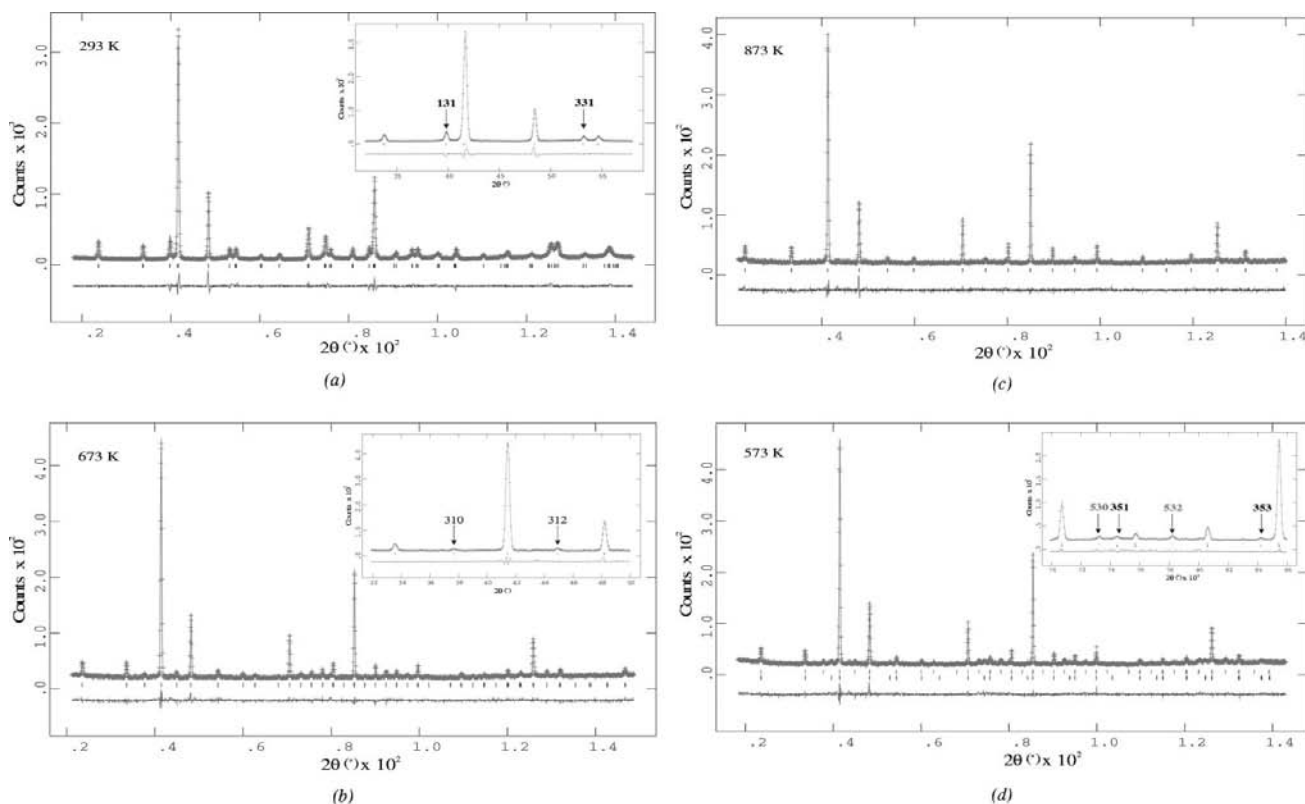
(b)

Atom	x	y	z	U^{11}	U^{22}	U^{33}	U^{12}	U^{13}	U^{23}
Rhombohedral phase (293 K)									
Na	0.0	0.0	0.2627 (6)	0.022 (3)	0.022 (3)	0.036 (9)	0.011 (2)	0.0	0.0
Bi	0.0	0.0	0.2627 (6)	0.036 (2)	0.036 (2)	0.091 (6)	0.018 (1)	0.0	0.0
Ti	0.0	0.0	0.0063 (6)	0.011 (2)	0.011 (2)	0.009 (3)	0.006 (1)	0.0	0.0
O	0.126 (1)	0.336 (1)	0.0833†	0.031 (3)	0.006 (1)	0.048 (1)	0.014 (3)	–0.004 (3)	–0.011 (1)
Tetragonal phase (673 K)									
Na	0.0	0.5	0.545 (2)	0.051 (6)	0.051 (6)	0.039 (2)	0.011 (1)	0.0	0.0
Bi	0.0	0.5	0.545 (2)	0.071 (3)	0.071 (3)	0.037 (6)	–0.002 (4)	0.0	0.0
Ti	0.0	0.0	0.0‡	0.014 (2)	0.014 (2)	0.014 (4)	0.0	0.0	0.0
O(I)	0.0	0.0	0.510 (3)	0.063 (2)	0.063 (2)	0.020 (3)	0.0	0.0	0.0
O(II)	0.271 (1)	0.229 (1)	0.015 (4)	0.024 (1)	0.024 (1)	0.056 (2)	–0.013 (1)	0.001 (3)	–0.001 (3)
Cubic phase (873 K)									
Na	0.0	0.0	0.0	0.077 (4)	0.077 (4)	0.077 (4)	0.0	0.0	0.0
Bi	0.0	0.0	0.0	0.077 (2)	0.077 (2)	0.077 (2)	0.0	0.0	0.0
Ti	0.5	0.5	0.5	0.022 (1)	0.022 (1)	0.022 (1)	0.0	0.0	0.0
O	0.5	0.5	0.0	0.062 (1)	0.062 (1)	0.012 (1)	0.0	0.0	0.0

† O(z) fixed to deal with floating origin. ‡ Ti(z) fixed to deal with floating origin.

distortion parameter d is not shown as it remained constant to within experimental error. As the sense of s and t has already been allocated, the sign of d is no longer arbitrary. The distortion remains negative over the temperature range, suggesting that the upper face of the octahedron is larger than the lower face. Coexistence of rhombohedral and tetragonal

phases, as indicated by the presence of both types of superstructure reflections (h odd, k odd, l odd and h odd, k odd, l even), were based on the nearest subsequent refinement model and refined together. The observed, calculated and difference profiles from the final Rietveld refinement in $R3c$ and $P4bm$ at 573 K are shown in Fig. 3(d). From numerical

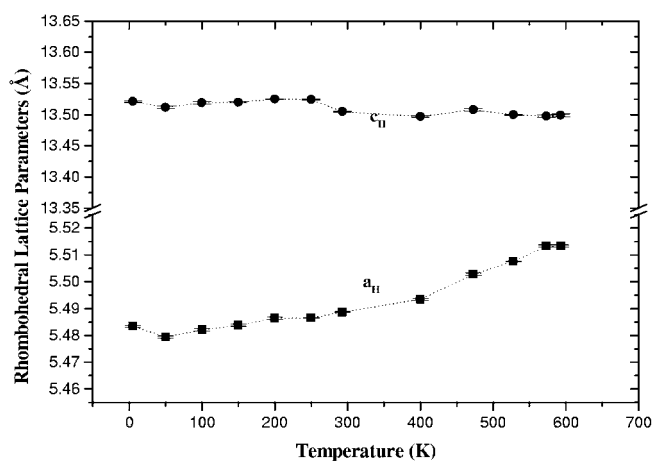

Figure 3

The observed, calculated and difference curves from the Rietveld refinement of $\text{Na}_{0.5}\text{Bi}_{0.5}\text{TiO}_3$. (a) Refinement in $R3c$, at 293 K; the marks indicate the positions of the reflections. The low-angle data ($32 < 2\theta < 58^\circ$) showing the first two superstructure peaks are magnified in the insert. (b) Refinement in $P4bm$, at 673 K; the low-angle data ($32 < 2\theta < 50^\circ$), showing the first two superstructure peaks, are magnified in the insert. (c) Refinement in $Pm3m$, at 873 K. (d) Refinement in $R3c$ and $P4bm$ – coexistence region at 573 K; the top and bottom marks indicate the positions of the tetragonal and rhombohedral reflections, respectively. The mid-angle data ($70 < 2\theta < 86^\circ$), showing the positions of rhombohedral (351 and 353) and tetragonal (530 and 532) superstructure peaks, are magnified in the insert.

analysis of the diffraction patterns the contribution of particular phases in the coexistence regions to the sample volume was found. These figures were used as the starting fraction for the coexistence in the refinements. Refinements showed little variation from these calculated fractional volumes.

3.2. Tetragonal phase: refinement and structural characterization

Compared with the pseudo-cubic powder pattern referred to on the $2a \times 2b \times 2c$ ($8 \times 8 \times 8 \text{ \AA}^3$) unit cell, superstructure reflections of the type h odd, k odd, l even were observed within the temperature range 573–793 K. These reflections are consistent with the tilt system $a^0a^0c^+$ and the tetragonal unit cell $2^{1/2}a \times 2^{1/2}b \times c$. The rotation of the octahedra associated with this system results in cell doubling in the [100] and [010] directions, but as successive octahedra are rotated in the same direction about [001] there is no doubling in this direction. A view of the structure down [001] showing the tilt system and in the [010] direction showing relative cation displacements are shown in Figs. 7(a) and 7(b), respectively. The refinements strategy can be found elsewhere (Jones & Thomas, 2000). The space group $P4bm$ was assigned and refinements were stable and converged quickly. The crystallographic data and the refined profile parameters are summarized in Table 2.


Figure 4

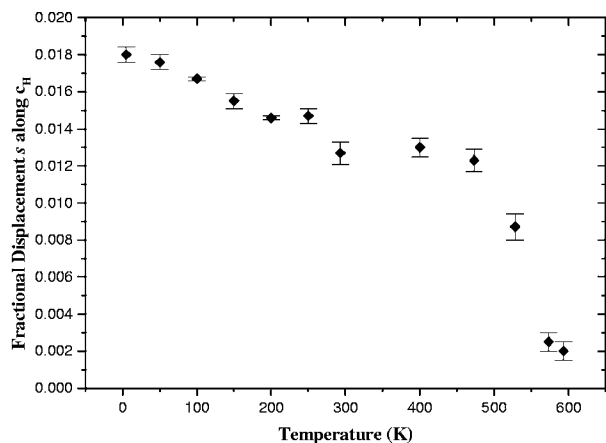
Variation of lattice parameters in the rhombohedral phase as a function of temperature.

It should be noted that the tetragonal phase of NBT was previously reported in space group $P4mm$ (Zvirgzds *et al.*, 1982). However, since the superstructure reflections arising from the octahedral tilts are absent in $P4mm$, this space group can be rejected on these grounds alone, in agreement with the assignment of the $a^0a^0c^+$ tilt system found by Soukhovjak *et al.*

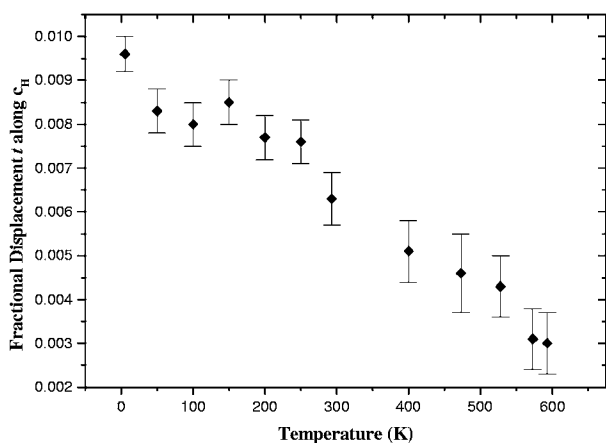
(2000). The observed, calculated and difference profiles from the final Rietveld refinement in $P4bm$ are shown in Fig. 4(b). Fig. 8(a) shows the trends in cation displacements obtained from refinements and Fig. 8(b) the variation in the tilt angle of the octahedron with temperature. Coexistence regions of the tetragonal and cubic phases were based on the nearest subsequent refinement models and refined together.

3.3. Cubic phases: refinement and structural characterization

The high-temperature paraelectric cubic form of NBT (space group $Pm\bar{3}m$) possesses no tilts or cation displacements. There was no evidence of cation ordering either from the neutron data here or from powder X-ray data taken at high temperature. The refinement was stable and converged quickly, the crystallographic data and the refined profile parameters are summarized in Table 2. The observed, calculated and difference profiles from the final Rietveld refinement are shown in Fig. 4(c). There is very little apparent



(a)

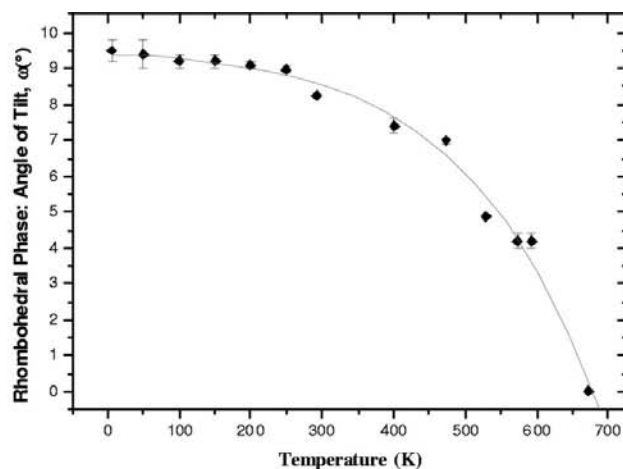


(b)

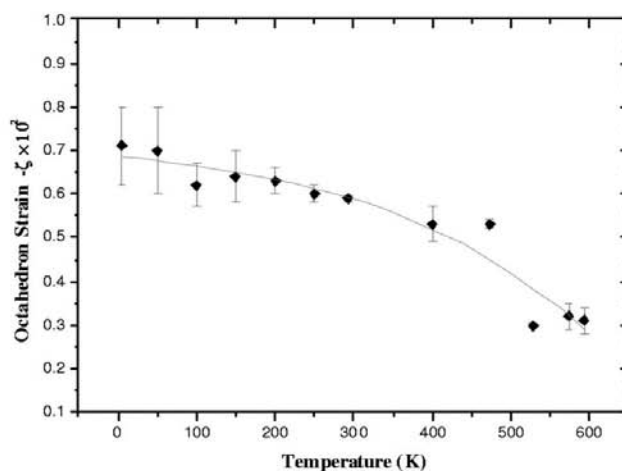
Figure 5

(a) The variation of Na/Bi cation shifts (expressed in fractions of c_H) with temperature; (b) the variation of Ti cation shifts (expressed in fractions of c_H) with temperature.

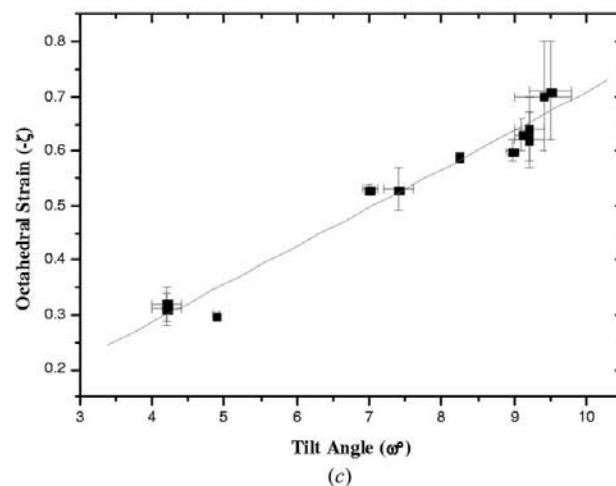
difference between the profiles in the coexistence tetragonal/cubic phase and the pure cubic phase, with the tetragonal superstructure reflections being very weak. Starting models



(a)



(b)



(c)

Figure 6

(a) Variation of the octahedron tilt angle ω with temperature; (b) variation of the octahedral strain ζ with temperature; (c) variation of octahedral strain ζ with tilt angle ω . The lines of best fit to the data act as guides to the eyes only.

for refinement in the coexistence region were based on the nearest subsequent refinement models and refined together.

3.4. SHG results

For the first time the SHG signal for NBT has been measured as a function of temperature, indicating that the tetragonal phase is indeed non-centrosymmetric and strengthening the proposition that the space group $P4bm$ is correct. Fig. 9(a) shows the normalized room-temperature SHG signal as a function of particle size displaying the non-

phase matchable nature of this material. The particle size range that gave the greatest signal was used to record the SHG signal between the temperature range 313–903 K; Fig. 9(b) shows the normalized signal within this temperature range. The dotted line marked by R represents the upper limit where the pure rhombohedral phase exists obtained from neutron diffraction data. Lines marked by T and C represent the beginning of the pure tetragonal and cubic phases, respectively, deduced from the neutron study.

4. Discussion

4.1. Lattice parameters and phase transitions

From the sequential refinements, the lattice parameters have been plotted in Fig. 10. The values of lattice parameters are comparable to those obtained by other authors, *e.g.* Suchanicz & Kwapulinski (1995) [slight variations that may exist can be attributed to material processing, as suggested by Park *et al.* (1994)]. Fig. 11 shows the pseudocubic unit-cell volume as a function of temperature. It is thought that the discrepancy in the linear progression of the volume is the result of an offset introduced by the different sample environments used, *i.e.* cryofurnace and high-temperature furnace. Fig. 12 shows the volumes of different phases as a function of temperature. The pure rhombohedral phase persists from 5 to

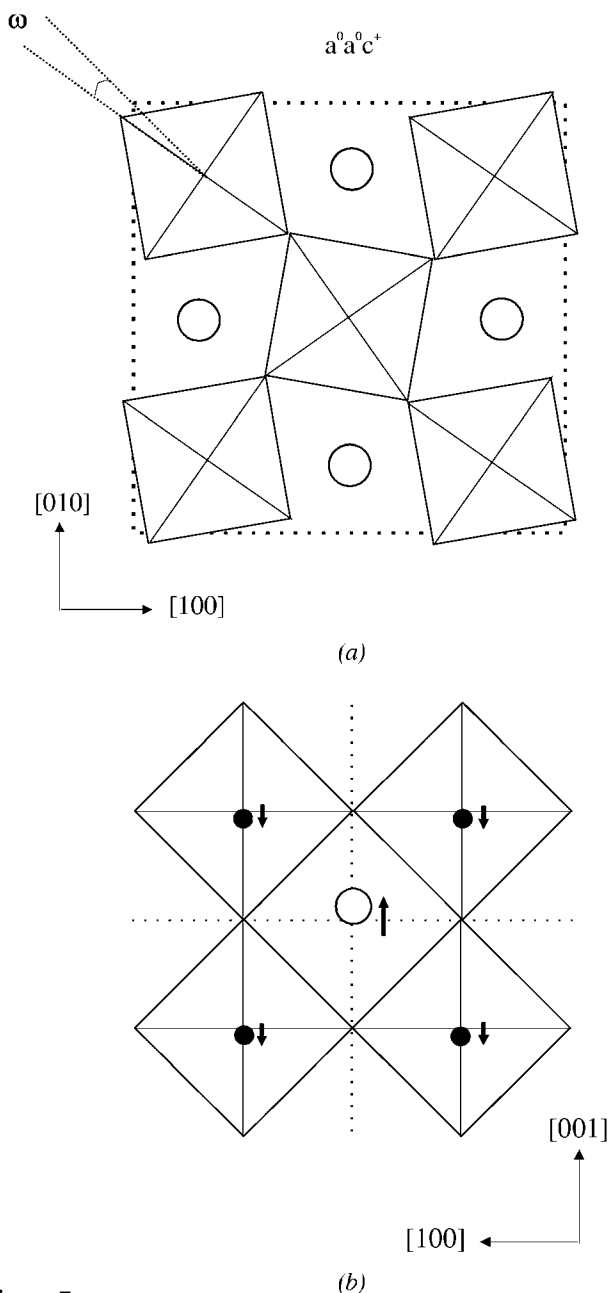


Figure 7
(a) The projection of the tetragonal structure down [001], open circles represent Na/Bi sites. (b) A view of the tetragonal structure along [010], showing the octahedral tilting about the polar c axis and the relative cation displacements. The open circles represent Na/Bi sites; smaller filled circles represent Ti sites.

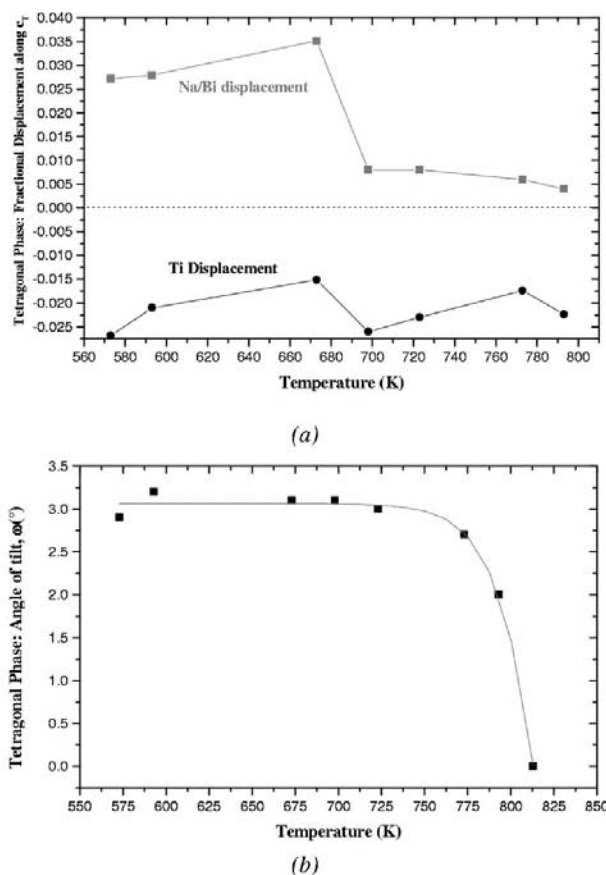


Figure 8
(a) The variation of cation shifts (expressed in fractions of c_T), with temperature; (b) the variation of octahedral tilt angle (ω , °) with temperature.

528 K, between 573–593 K a coexistence region can be seen and from 673–773 K the pure tetragonal phase occurs. Due to a limit in the time available for measurements, the regions 528–573 and 593–673 K could not be investigated more fully. As a result the extent over which the rhombohedral/tetragonal coexistence region lies could not be established more precisely. The tetragonal/cubic coexistence region lies between 773 and 813 K, with the pure cubic phase occurring at 813 K. These results are in close agreement with Suchanicz & Kwapulinski (1995) who carried out single-crystal X-ray measurements between 853 and 473 K on cooling. They found the pure cubic/tetragonal coexistence phase occurs between 813 and 773 K, and the rhombohedral/tetragonal coexistence region between 693 and 533 K. There is much contention associated with the rhombohedral/tetragonal coexistence phases within the literature. Some authors suggest that an antiferroelectric order exists between the rhombohedral/tetragonal phase (Kuharungrong & Schulze, 1996); however,

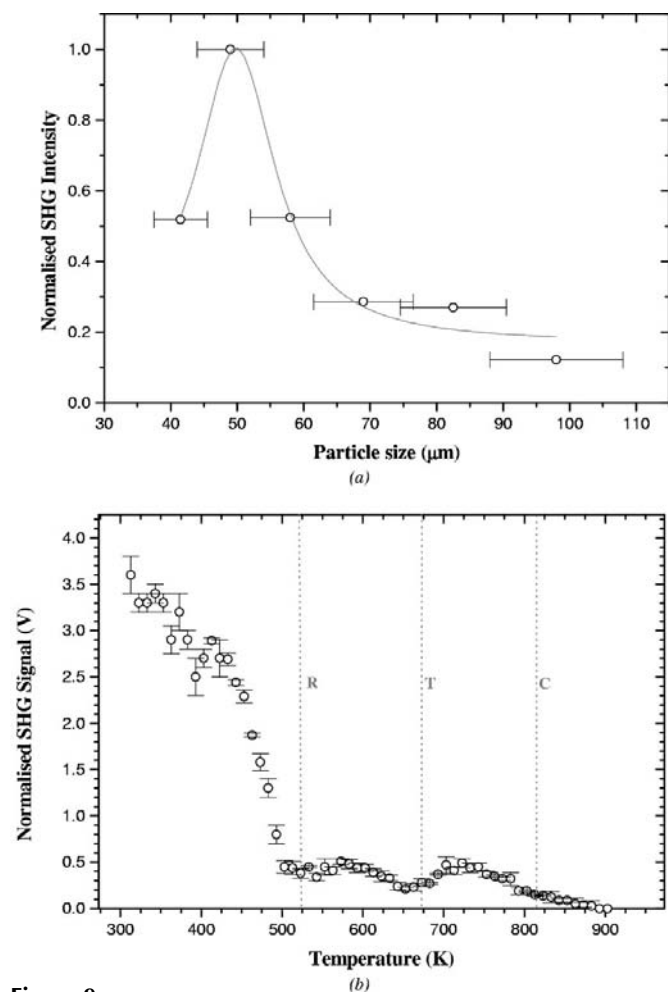


Figure 9
(a) Normalized particle size dependence of second harmonic intensity, non-phased matched for $\text{Na}_{0.5}\text{Bi}_{0.5}\text{TiO}_3$. The red line represents a Voigt fit to the data and is included as a guide for the eyes. (b) Second harmonic signal in $\text{Na}_{0.5}\text{Bi}_{0.5}\text{TiO}_3$ as a function of temperature. The red dotted lines marked R, T and C represent the onset of the rhombohedral, tetragonal and cubic regions obtained by neutron diffraction refinements. The SHG data have been normalized to the laser power output.

many investigations including this one do not show any evidence of long-range antiferroelectric order. Suchanicz & Kwapulinski (1995) found the rhombohedral/tetragonal coexistence range to be 160 K, but the results from Zvirgzds *et al.* (1982) found the range to be around 55 K. The results from this study suggest an upper temperature limit for this region of 145 K, but it is probably smaller. The major differences

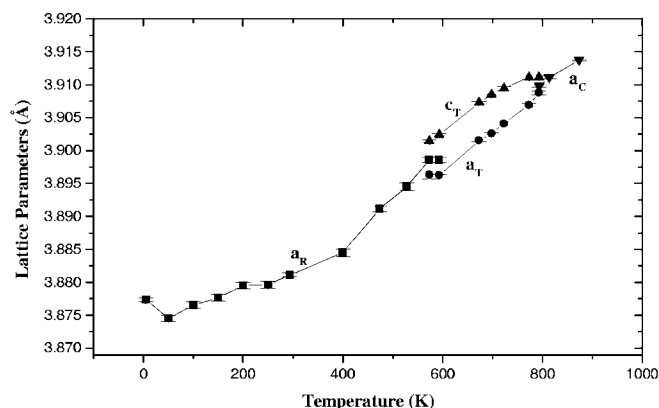


Figure 10
Lattice parameter evolution as a function of temperature; a_R refers to the rhombohedral lattice parameter, a_T to the tetragonal lattice parameter a , c_T to the tetragonal lattice parameter c and a_C to cubic lattice parameter a .

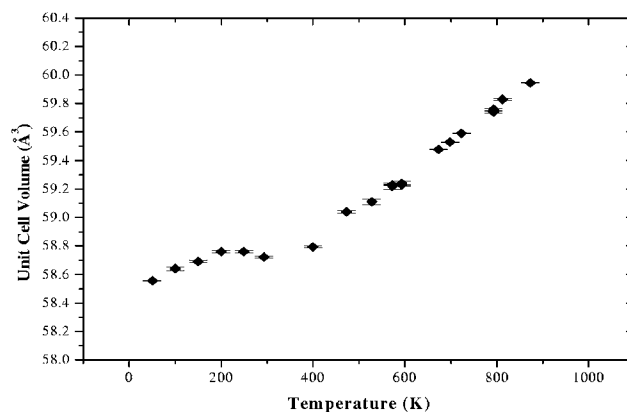


Figure 11
Pseudocubic unit-cell volume as a function of temperature.

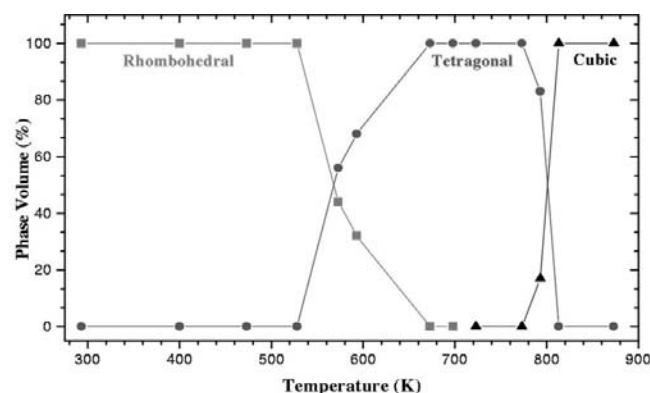


Figure 12
Percentage phase volumes as a function of temperature.

between these results and Suchanicz & Kwapulinski (1995) are in the temperatures at which the pure rhombohedral and tetragonal phases are first seen. Both the values obtained from this study are lower (by 5 and 20 K for the rhombohedral and tetragonal phases, respectively), an effect which could be explained by heating/cooling hysteresis effects.

The low-temperature profile differed from the room-temperature profile only in the positions of the reflections, accounted for by the change of lattice parameters at lower temperature. The relative intensities did not differ appreciably from those at room temperature. All reflections associated with the superstructure were observed down to 5 K. Suchanicz *et al.* (1998) have previously speculatively reported a phase transition at 55 K. There is a slight anomaly in the lattice parameters in this region (Fig. 5).

In order to investigate the phase transition temperatures more closely and to verify the non-centrosymmetric symmetry of the tetragonal phase, second harmonic generation was employed. Fig. 9(b) shows the phase transition behaviour in NBT. Structural transitions can be distinguished through changes in the intensity and the overall disappearance of an SHG signal. The plot indicates that changes occur in the regions roughly associated with phase transition regions obtained from the neutron data. The cubic phase indicated by zero output appears at 893 K, a shift from the neutron observation of 80 K. Signal intensity variations suggest transitions take place around 500 and 650 K, presumably these are associated with the rhombohedral/tetragonal coexistence and tetragonal phase transitions. The fact that there is a signal over the tetragonal phase region supports the assignment of the non-centrosymmetric space group $P4bm$.

4.2. Cation ordering

It is known that cation ordering in complex B-site substituted perovskites is driven by fundamental factors such as ion size and charge (Setter & Cross, 1980). Compounds that possess sufficiently large differences in the size of the B-cations are driven strongly towards ordering by electrostatic forces, whereas materials with closely matched cation sizes are nearly always disordered. Similarly, large variations in the valence between B cations results in a powerful tendency towards ordering through electrostatic forces. There are relatively few examples of A-cation ordering, due mainly to the overall limited number of compounds existing and it would not be unreasonable, however, to presume that similar ordering arguments hold for A-substituted complex perovskites.

Park *et al.* (1999) have shown through diffraction studies that a partial ordering of the $\text{Nd}^{3+}/\text{Ag}^+$ cations occur in the A-site substituted perovskite $\text{Nd}_{0.5}\text{Ag}_{0.5}\text{TiO}_3$. This layered A-site ordering is driven by the charge and size difference between Nd^{3+} and Ag^+ , where the difference in ionic radii is $\Delta_{\text{Nd}/\text{Ag}} = 0.171 \text{ \AA}$. There have also been reports of long-range cation ordering in NBT. Park *et al.* (1994) in single-crystal rotation camera experiments found a low degree of $\text{Na}^+/\text{Bi}^{3+}$ ordering

and suggested an ordered face-centred structure (space group $Fm\bar{3}m$) for the high-temperature cubic phase.

No superstructure peaks associated with cation ordering have been observed in NBT, either in X-ray or neutron experiments. From the point of view of differing size mechanisms, as the ionic radii difference in NBT is close to zero (Shannon, 1976) and the $(\text{Na}/\text{Bi})\text{O}_{12}$ cuboctahedra are approximately the same size, no long-range ordering would be expected. Long-range order is also absent in NBT's analogue, $\text{Ag}_{0.5}\text{Bi}_{0.5}\text{TiO}_3$, where $\Delta_{\text{Ag}/\text{Bi}} = 0.11 \text{ \AA}$ (Park *et al.*, 1999). Na/Bi cations distribute at sites randomly and the high-temperature (813 K and above) structure is therefore a primitive cubic structure with space group $Pm\bar{3}m$. There does, however, remain the possibility that short-range ion order exists in NBT. This is manifested as weak diffuse scattering and is revealed by Raman spectroscopy, which indicates Na/Bi clustering (Kreisel *et al.*, 2000).

4.3. Octahedral tilting and cation displacements

As temperature is decreased NBT distorts from the ideal prototypic cubic perovskite structure by octahedral tilting. Tetragonal superstructure reflections are seen to appear then diminish, with rhombohedral superstructure reflections appearing with a further temperature decrease. Fig. 13 shows the variation in intensity of the $(5\bar{1}3)$ rhombohedral and (532) tetragonal superstructure peaks relative to the main (424) peak. Octahedral tilting is driven by the need to optimize the anion coordination about the A cation. Since Bi^{3+} and Na^+ are relatively small cations in the A-site, the presence of octahedral tilts is expected. For example, the $a^-a^-a^-$ (Megaw & Darlington, 1975) and $a^0a^0c^+$ (Glazer & Megaw, 1972) tilt systems both occur in NaNbO_3 and $a^-a^-a^-$ is also found in BiFeO_3 (Megaw & Darlington, 1975).

The tetragonal structure is distorted from cubic by in-phase rotations of the TiO_6 octahedra about the c axis, combined with antiparallel displacement of the cations along the polar c axis (Jones & Thomas, 2000). The $a^0a^0c^+$ tilts in this structure

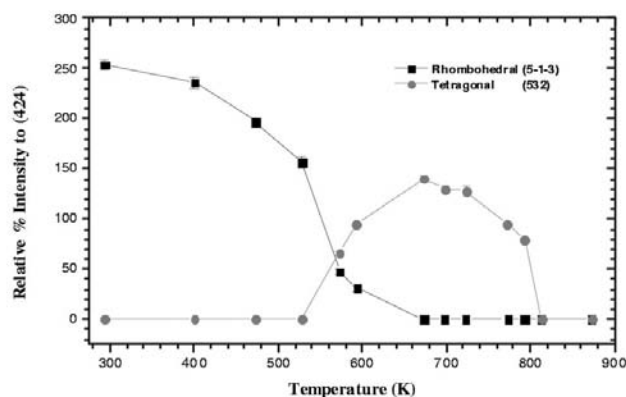


Figure 13 Variation in intensity of $(5-1-3)$ and (532) superstructure peaks relative to (424) main peak.

produce an indistinguishable environment for the A-cation when viewed (from the cation) along $+c$ and $-c$. Therefore, from the geometry of the framework alone, there is no incentive for the A cation to move off-centre. Since A-cation displacements along [001] are not driven by the octahedral tilts, the conclusion that they result from the need to accommodate the stereoactive lone pair on Bi^{3+} has previously been reached (Jones & Thomas, 2000). The electronic configuration of Bi^{3+} is the same as that of Pb^{2+} (both having a completed outer 6s shell), which is likewise a lone-pair cation. Thomann (1987) noted the tendency of Bi^{3+} to behave similarly to Pb^{2+} in perovskites and identified Bi^{3+} as a cation likely to promote ferroelectric structures. The tetragonal phase of PbTiO_3 (space group $P4mm$) has Pb^{2+} cations displaced 0.47 Å along the c axis (Glazer *et al.*, 1978), although the framework is not tilted as expected for the larger Pb^{2+} ion. This is in contrast with the isostructural material BaTiO_3 where the Ba displacement is only 0.07 Å (Shirane *et al.*, 1955). Within the tilted framework, even though there is no geometric impetus for the cations to move off-centre, the inherent properties of Bi^{3+} promote movement along the polar axis, thus generating this unusual structure. It should be noted, however, that Bi^{3+} and Ti^{4+} are displaced in opposite directions along $+c$ to establish a locally non-polar (ferrielectric) arrangement in the unit cell; indeed, a simple point-dipole model gives a spontaneous dipole moment of almost zero. Thus, although the freedom of the polar space group $P4bm$ was necessary for refinement, the tetragonal structure is weakly polar, as also indicated by the small SHG signal.

Fig. 8(a) shows the Na/Bi and Ti refined shifts plotted as a function of temperature for the tetragonal phase of NBT. The overall displacement of cations calculated in the Rietveld refinements are from the centre of their coordination polyhedra. A- and B-cation displacements are in opposite directions, both being directed along the polar c axis. A view of the structure down [001] showing the tilt system and in the [010] direction showing relative cation displacements are shown in Figs. 7(a) and 7(b), respectively. Within the tetragonal phase region Na/Bi displacements are seen to follow a gradual rise followed by a quite rapid drop over a narrow temperature range and then a moderate displacement decrease as a function of increasing temperature. Ti displacements are anti-parallel to Na/Bi displacements and show a relatively constant progression with temperature. Fig. 8(b) shows the evolution of the octahedral tilt angle ω with temperature. This varies modestly over a wide temperature region then drops to zero when the transition to the cubic phase occurs and the oxygen octahedra are no longer rotated.

The rhombohedral structure of NBT is described by the polar space group $R3c$, with $a^-a^-a^-$ antiphase rotations of the TiO_6 octahedra about the pseudo-cubic axes. A- and B-cation displacements are parallel to each other, which in turn are parallel to $[111]_p$ (the shifts of the O atoms are also in the same direction). Displacement of the A-site cations along $[111]_p$ result from a need to achieve electrostatic energy minimization associated with the tilting octahedra and also are

presumably driven (to a differing extent) by the need to accommodate the stereoactive lone pair on Bi^{3+} .

Figs. 5(a) and 5(b) show the Na/Bi (s) and Ti (t) fractional displacements along c_H plotted as a function of temperature for the rhombohedral phase of NBT. A view of the structure down [001] showing the tilt system is shown in Fig. 2. The overall displacement of cations calculated in the Rietveld refinements are from the centre of their coordination polyhedra.

The overall trend in s and t shows a decrease of displacement with increasing temperature. This is expected and brought about by the contraction of the c_H axes and elongation of the a_H axes with increasing temperature (consequently the c/a ratio decreases giving rise to decreases in Na/Bi and Ti relative to the oxygen octahedron). At lower temperatures the fractional displacement of the Na/Bi cations is approximately twice that of Ti displacement, but at the higher temperatures where the phase is changing to one of tetragonal symmetry these displacements become comparable. The displacement progression with temperature is markedly different for the cation types. The Ti displacements gradually decrease in a linear manner with temperature. Na/Bi displacements decrease linearly until 573 K (coexistence region), when there seems to be a greater relative change resulting in comparable displacement values with Ti at that temperature. The Na/Bi displacements up to this temperature are approximately twice that of Ti displacements, a similar displacement trend can be seen in the B-site substituted perovskite PZT (Glazer *et al.*, 1978), with the shift of the A cation being 1.5 times that of the B cation.

Fig. 6(a) shows the thermal evolution of the experimentally determined tilt angle ω . It clearly shows a continual decrease in the octahedron tilting with increasing temperature. The Na/Bi (s) displacement variation with temperature decreases in the same manner, indicating the mutual nature of these parameters. The lines of best fit to the data act as guides to the eyes only. The room-temperature octahedral tilting angle estimated from oxygen fractional coordinates was found to be $8.24(4)^\circ$. In contrast, the NaNbO_3 (at 123 K) $a^-a^-a^-$ tilt system has an octahedral tilting angle equal to 12.1° (Megaw & Darlington, 1975) and $\text{Ag}_{0.5}\text{Bi}_{0.5}\text{TiO}_3$, which shows anti-phase rotations about the z axes; tilt system $a^0a^0c^-$ has a tilting angle of $8.91(1)^\circ$ (Park *et al.*, 1999).

The tilt angle and the hexagonal cell parameters are coupled through an additional parameter called the octahedral strain ζ (Megaw & Darlington, 1975), where the factor $1 + \zeta$ is the elongation ($\zeta > 0$) or compression ($\zeta < 0$, $\zeta = 0$ for unstrained octahedra) of the octahedron along c_H . They found that for many of the perovskite-type structures the octahedral strains are generally negative and decrease when the tilt angle decreases. The evolution of the experimentally determined octahedral strain ζ with temperature, calculated from the unit-cell dimensions, is shown in Fig. 6(b). It shows a gradual fall with increasing temperature similar to the tilt-angle progression. The sign of the octahedral strain ζ is negative, signifying that a flattening of the octahedral units occurs. Fig. 6(c) shows

the relationship between octahedral strain ζ and tilt angle ω , indicating a generally linear relationship.

4.4. Valency calculations

A valency deficiency gives rise to a displacement of the cation. The cation moves off-centre in order to achieve a valency closer to its ideal value. Bond-valence calculations for the room-temperature rhombohedral and high-temperature cubic phases were performed using the program *VaList* (Willis & Brown, 1999). With the cations at their refined positions (or fixed positions in the cubic case), values obtained for Na^+ and Ti^{4+} showed a 6 and 2% difference for the rhombohedral phase and 11 and 2% difference for the cubic phase, from their ideal values. However, the bond-valence sum calculated for Bi^{3+} for the rhombohedral and cubic phases showed a 22 and 35% deficiency, respectively, from its ideal value of 3.0. In the rhombohedral (*R3c*) phase of BiFeO_3 , Bi^{3+} has a valence deficiency of 13%, despite a displacement along the polar axis, to distort its coordination, as large as 0.62 (3) Å (Moreau *et al.*, 1971). Displacement of Bi^{3+} and valence deficiency was also seen in the orthorhombic phase of $\text{Ag}_{0.5}\text{Bi}_{0.5}\text{TiO}_3$ (Park *et al.*, 1999) and in the tetragonal phase of NBT (Jones & Thomas, 2000) with Bi^{3+} showing a 26 and 32% deficiency, respectively, from its ideal value.

Even though Bi^{3+} moves off-centre in order to satisfy its own stereochemical preferences, on the A site of perovskite structures in rhombohedral, tetragonal and orthorhombic polar phases, it seems that it is unable to achieve a perfect match to its valency. It is clear that the character of the bismuth cation plays an important role in determining displacements. The fact that no displacements are observed in the analogue $\text{Nd}_{0.5}\text{Ag}_{0.5}\text{TiO}_3$ strengthens this idea.

5. Conclusions

Structural investigations of the phases occurring in the compound NBT within the 5–873 K temperature range using neutron powder diffraction have been carried out. This technique is sensitive to oxygen positions and has yielded much information, especially in relation to the octahedral deformations and their systematic behaviour with temperature. General trends of cation displacements and the various deviations of the octahedral network from the prototypic cubic perovskite structure have been established.

In summary, between 5 and 593 K the phase is rhombohedral (*R3c*) with the pseudo-cubic perovskite cell axes doubled. In this phase the Na/Bi and Ti atoms are displaced parallel to each other along [111] to give a polar ferroelectric phase. At the same time, the oxygen octahedra are tilted about [111] with antiphase ($a^-a^-a^-$) tilts, giving rise to the doubling of the unit-cell axes. At 593 K the tetragonal phase of NBT (*P4bm*) is observed. In this phase Na/Bi and Ti atoms are displaced in opposite directions along the polar [001] axes, combined with in-phase ($a^0a^0c^+$) tilts of oxygen octahedra, resulting in cell doubling in the [100] and [010] directions.

Finally at around 813 K the cation displacements and tilt systems disappear to give the ideal cubic perovskite structure. Coexistence regions of a broad rhombohedral/tetragonal and tetragonal/cubic phase exist. No clear evidence for ordering or a low-temperature phase transition has been found.

The authors wish to thank A. W. Hewat and P. Cross for their help at the Institut Laue–Langevin (ILL), with the neutron experiments. This research has been funded by an Engineering and Physical Sciences Research Council (EPSRC) Studentship award.

References

- Corker, D. L., Glazer, A. M., Whatmore, R. W., Stallard, A. & Fauth, F. (1998). *J. Phys. Condens. Matter*, **10**, 6251–6269.
- Glazer, A. M. (1975). *Acta Cryst.* **A31**, 756–762.
- Glazer, A. M., Mabud, S. A. & Clarke, R. (1978). *Acta Cryst.* **B34**, 1060–1065.
- Glazer, A. M. & Megaw, H. D. (1972). *Philos. Mag.* **25**, 1119–1135.
- Isupov, V. A. & Kruzina, T. V. (1983). *Izv AN SSSR Ser. Fiz.* **47**, 616–619.
- Jones, G. O. & Thomas, P. A. (2000). *Acta Cryst.* **B56**, 426–430.
- Kreisel, J., Glazer, A. M., Jones, G. O., Thomas, P. A., Abello, L. & Lucazeau, G. (2000). *J. Phys. Condens. Matter*, **12**, 3267–3280.
- Kuharungrong, S. & Schulze, W. (1996). *J. Am. Ceram. Soc.* **79**, 1273–1280.
- Kurtz, S. K. & Perry, T. T. (1968). *J. Appl. Phys.* **39**, 3798–3813.
- Megaw, H. D. & Darlington, C. N. (1975). *Acta Cryst.* **A31**, 161–173.
- Moreau, J. M., Michel, C., Gerson, R. & James, W. J. (1971). *J. Phys. Chem. Solids*, **32**, 1315–1320.
- Park, J. H., Woodward, P. M. & Parize, J. B. (1998). *Chem. Mater.* **10**, 3092–3100.
- Park, J. H., Woodward, P. M., Parize, J. B., Reeder, R. J., Lubomirsky, I. & Stafussd, O. (1999). *Chem. Mater.* **11**, 177–183.
- Park, S., Chung, S., Kim, I. & Hong, K. S. (1994). *J. Am. Ceram. Soc.* **77**, 2641–2647.
- Setter, N. & Cross, L. E. (1980). *J. Mater. Sci.* **15**, 2478–2482.
- Shannon, R. D. (1976). *Acta Cryst.* **A32**, 751–767.
- Shirane, G., Pepinsky, R. & Frazer, B. C. (1955). *Phys. Rev.* **97**, 1179.
- Smolenskii, G. A., Isupov, V. A., Agranovskaya, A. I. & Krainik, N. N. (1960). *Sov. Phys. Solid State*, **2**, 2982–2985.
- Soukhovjak, A. N., Wang, H., Farrey, G. W. & Chiang, Y.-M. (2000). *J. Phys. Chem. Solids*, **61**, 301–304.
- Suchanicz, J., Jezowski, A. & Poprawski, R. (1998). *Phys. Statua Solidus*, **169**, 209–215.
- Suchanicz, J. & Kwapulinski, J. (1995). *Ferroelectrics*, **165**, 249–253.
- Suchanicz, J. & Ptak, W. S. (1990). *Ferroelectric Lett.* **12**, 71–78.
- Thomann, H. (1987). *Ferroelectrics*, **73**, 183–199.
- Tu, C., Siny, I. & Schmidt, V. (1994). *Phys. Rev. B*, **49**, 11550–11559.
- Vakhrushev, S. B., Isupov, V. A., Kvyatkovsky, B. E., Okuneva, N. M., Pronin, I. P., Smolenskii, G. A. & Syrnikov, P. P. (1985). *Ferroelectrics*, **63**, 153–160.
- Vakhrushev, S. B., Kvyatkovskii, B. E., Malysheva, R. S., Okuneva, N. M. & Syrnikov, P. P. (1989). *Kristallografiya*, **34**, 154–158.
- Von Dreele, R. & Larson, A. (1995). *GSAS*. Los Alamos National Laboratory, New Mexico, USA.
- Willis, A. S. & Brown, I. D. (1999). *VaList*. CEA, France.
- Woodward, P. M., Vogt, T., Cox, D. E., Arulraj, A., Rao, C. N. R., Karen, P. & Cheetham, A. K. (1998). *Chem Mater.* **10**, 3652–3665.
- Zvirgzds, J. A., Kapostins, P. P., Zvirgzde J. V. & Kruzina, T. V. (1982). *Ferroelectrics*, **40**, 75–77.